Rakenteiden Mekaniikka (Journal of Structural Mechanics) Vol. 58, No. 3, 2025, pp. 132–154 http://rakenteidenmekaniikka.journal.fi https://doi.org/10.23998/rm.157104



© 2025 The Authors

Open access under the license CC BY 4.0

# Asymmetric constant-stress arch shape in tied-arch bridges

Esko Järvenpää<sup>1</sup> and Anssi Laaksonen

**Summary** This study focuses on the asymmetric, momentless, constant-stress form of the arch in tied-arch bridges. The most common asymmetric shape of arch bridges is caused by variations in the heights of the abutments that support them. In recent years, a number of arch bridges with asymmetrical arches have been constructed, creating distinctive and intriguing aesthetics. This article proposes a methodology for optimally designing an asymmetric arch. The use of inclined parallel hangers is demonstrated to facilitate the creation of a pleasing, moment-free, constant stress tied-arch shape. The method used to calculate the shape of a tied-arch under constant stress is verified by finite element analysis. The primary objective of this paper is to demonstrate that an asymmetrical shape can be a structurally viable option without incurring excessive additional costs.

Keywords: arch, asymmetric arch, constant-stress arch

Received: 18 February 2024. Accepted: 22 October 2025. Published online: 24 October 2025.

#### Introduction

Historically, the configuration of the arch was a key consideration in stone arch construction. Bridge builders were already familiar with the concept of the thrust line. However, advances in materials and design tools have changed this. Arch spans have increased considerably, and the increased use of modern computer-aided design and analysis methods has resulted in a decline in focus on fundamental structural mechanics. Consequently, it may be advisable to place greater emphasis on the significance of conceptual design [1].

The conventional design principle for masonry arches is that the thrust line should be within the inner third of the arch's cross-section, to avoid tensile stresses [2]. However, this principle is too loose for steel and concrete arches, as it is particularly important to determine the optimum shape in order to minimise bending moments more accurately. In the case of bridges, traffic loads induce almost equal maximum compressive and tensile

<sup>&</sup>lt;sup>1</sup>Corresponding author: eojarvenpaa@gmail.com

bending stresses in the arch, and the same also occurs in the tie girder [3]. Therefore, the permanent load case closely approximates the optimum case for determining the arch's shape, thereby minimising the influence of traffic loads on the structural dimensions. The optimum shape of the centre of gravity axis of the arch eliminates bending moments caused by the eccentricity of significant compressive forces within the arch rib. This principle of axial force line location applies to asymmetric arches.

In conventional design practice, arches have been designed using symmetrical geometric shapes such as circles, parabolas, catenary curves and ellipses. The development of sophisticated calculation software has made it possible to routinely calculate stresses in arch structures. However, the optimal arch shape and potential for improvement have not been given due consideration, despite the fact that momentless permanent loading can significantly improve the arch's feasibility. Concerns have been raised about the structural integrity and economic viability of asymmetric arches. This article presents a method for designing asymmetric, momentless, constant-stress tied-arch bridges. The amount of material required is compared with that required for symmetrical arches.

Basic statics and vector algebra solutions using the numerical iterative method are an effective and practical tool for finding moment-free arch shape, as the loads are not limited to the self-weight and uniformly distributed loads.

# Asymmetry caused by terrain topography and road geometry

A common factor responsible for the formation of an asymmetric arch profile is the topography of the bridge site, which results in different heights of the bearing lines of the arch, as shown in Figure 1.

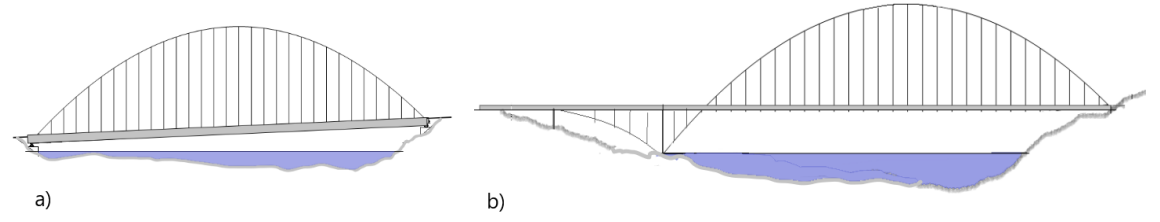


Figure 1. Asymmetric arch profiles: (a) Different bearing lines levels in tied-arch bridge. (b) Considerable difference in bearing line levels in arch bridge.

# Location of the apex of an asymmetric arch under a uniform vertical load

The following case is based on the assumption that the arch carries a uniformly distributed vertical load of w from the deck, including the weight of the tie. This can be interpreted as a situation in which the arch and hanger cables have zero weight. The shape of the momentless arch is parabolic. However, it should be noted that this loading assumption is not applicable to real bridges and should be considered an approximation.

The following figure illustrates the case of a weightless asymmetric arch for a vertical uniform load. Figure 2(a) shows the horizontal force H replacing the force of the tie, and Figure 2(b) shows the respective free body diagrams of the arch segments.

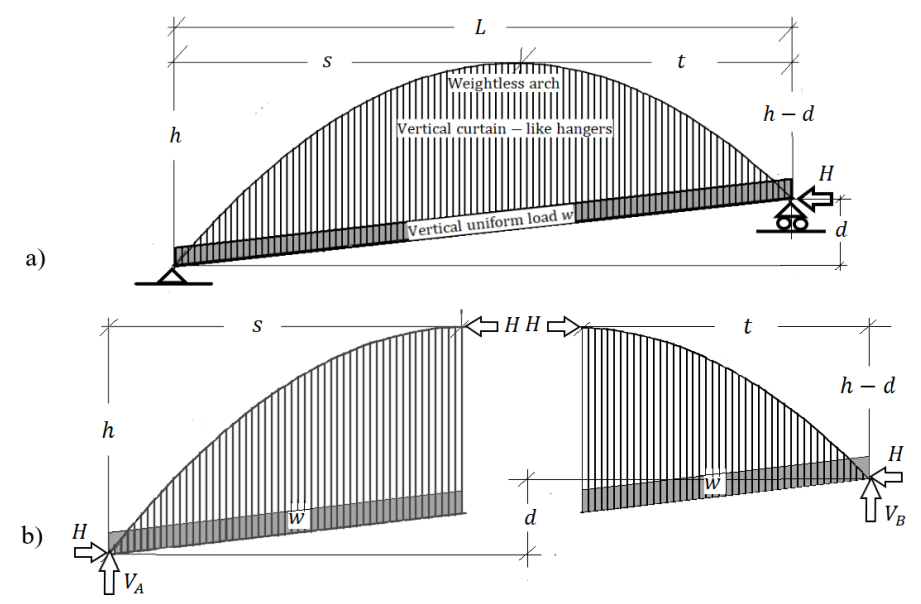


Figure 2. (a) Arch with different bearing line levels. (b) Free body drawing of the arch to carry the load w.

Using the symbols shown in Figure 2, the apex position of the arch can be calculated from the equilibrium as

$$H = \frac{ws^2}{2h} = \frac{wt^2}{2(h-d)}. (1)$$

Substituting t = L - s gives the expression

$$s^2d - 2sLh + L^2h = 0, (2)$$

which, when solved for s, gives the location of the apex as:

$$s = \frac{L(h - \sqrt{h^2 - dh})}{d}.$$
 (3)

The support reactions  $V_A$  and  $V_B$  are given by the equations

$$V_A = \frac{wL}{2} + \frac{Hd}{L}$$
 and  $V_B = \frac{wL}{2} - \frac{Hd}{L}$ . (4)

In the absence of definitive permanent load distribution data, Equation (3) can be used to provide a rough preliminary estimate of the apex position. The balanced shape of the arch of the Chenab Bridge in India is used to illustrate this. The arch is slightly asymmetric due to the challenging terrain at the bridge's location. Figure 3(a) shows the position of the apex in the final bridge design, with dimension *s* measuring 238.5 m [4].

Substituting the values L = 467.0 m, h = 120.0 m and d = 15.0 m into Equation (3) yields a value of s of 241.3 m. The difference between the approximate apex position obtained using Equation (3) and the final dimension s is 2.8 m.

Figure 3(b) shows the dimensions of the Yeshan River Bridge in China [5]. The apex distance *s* is 70.4 m, whereas the corresponding value obtained using Equation (3) is 69.8 m, resulting in a difference of 0.6 m.

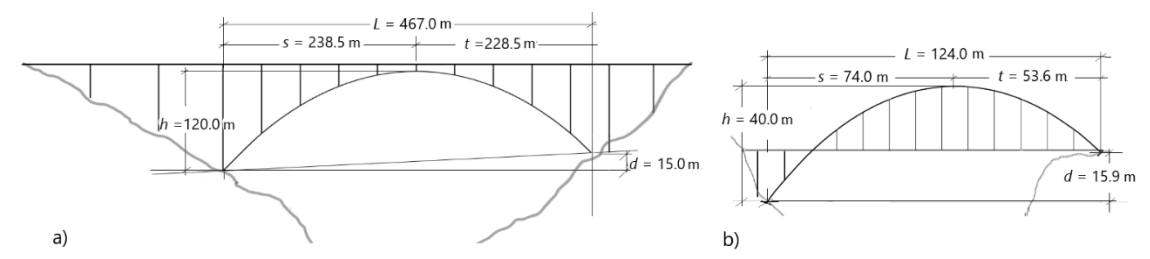


Figure 3. Apex positions: (a) Chenab Bridge. (b) Yeshan River Bridge.

## Momentless shape and position of the apex for overall permanent loads

Taking the weight of the arch bars, tie and hangers into account when finding the momentless shape of the arch leads to an iterative calculation. The new shape also changes the position of the apex compared to that calculated for a parabolic arch with only a uniform deck load. The next chapter discusses iteration using spreadsheet calculation and vector algebra as a simple method for preliminary design.

# Asymmetric anti-funicular shape of vertical hanger arch bridge

The conventional approach of using drafting techniques to determine the precise geometry of an arch without bending moments is no longer adequate for achieving the desired level of accuracy. Applying graphical statics in the form of vector algebra calculation solves this problem [6]. The proposed method enables the shape of the arch to be calculated according to the load distribution of the real bridge.

At the start of the calculation, the deck weight, span length, arch height, selected stresses for the arch, hanger cables and tie, and material densities are entered. During the iteration rounds, the coordinates of the arch and the cross-sections, as well as the weights of the hangers and the tie structure, are dimensioned.

Equation (3) can be used to determine the initial position of the apex for the weightless arch. However, the position of the apex will change due to the weight of the arch.

A practical iterative solution for a tied-arch bridge structure can be found by dividing the arch into two segments at the apex. Figure 4 shows an asymmetric tied-arch split into two free-body diagrams, with the nodal points of the deck and arch indicated. The distances s and t of the apex are defined when the horizontal forces H, calculated from both arch segments, are equal.

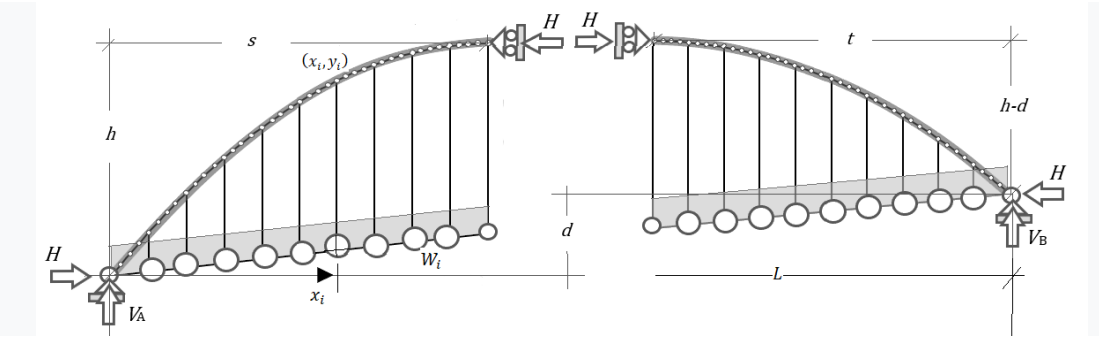


Figure 4. Free body drawing of an asymmetric tied-arch with vertical hangers.

As shown in Figure 5, the arch calculation model comprises nodes and straight bars connecting them. Node numbers start from 0 and bar numbers from 1, with both ending at n.

The arch is loaded with point loads applied to the nodes. The deck load, denoted  $W_{di}$ , and the load due to the tie weight, denoted  $W_{ti}$  in Figure 5, are equivalent vertical point loads conveyed to the arch's nodes by vertical hangers. The point loads are due to the weight of the arch, denoted  $W_{ai}$  and the weight of hangers denoted  $W_{hi}$ . At the node points between the hangers, only the arch's self-weight is valid. Figure 5 shows the weights of the tie and hangers in brackets because, for the purposes of further calculations, it is assumed that the weight of the tie is included in that of the deck and that the hangers are weightless.

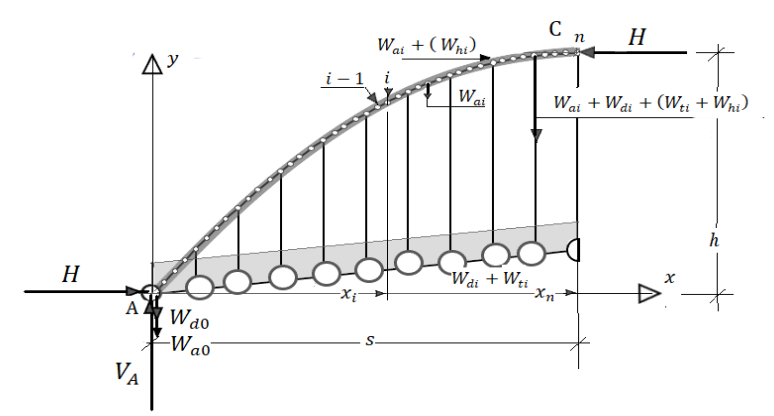


Figure 5. Free body diagram of a segment AC of an asymmetric tied-arch with vertical hangers.

Numbering of bars, nodes and nodal loads.

The distributed load of the arch within the bar i is assumed to be constant  $w_{ai}$ . The equivalent loads  $W_{ai}^l$  and  $W_{ai}^r$  at bar ends at the left (l) and right (r) of the bar i are

$$W_{ai}^{l} = W_{ai}^{l} = \frac{w_{ai}\Delta x_{i}}{2} \quad i = 1, ..., n,$$
 (5)

where  $\Delta x_i = x_i - x_{i-1}$  as shown in Figure 6(a). Equivalent nodal loads are obtained from the bar end loads using equations

$$W_{a0} = W_{a1}^l, \quad W_{ai} = W_{ai}^r + W_{ai+1}^l \quad i = 1, ..., n-1, \quad W_{an} = W_{an}^r.$$
 (6)

If the nodes are horizontally equally spaced ( $\Delta x_i = \Delta x = \text{constant}$ ) the result is

$$W_{a0} = w_{a1} \frac{\Delta x}{2}$$
,  $W_{ai} = (w_{ai} + w_{ai+1}) \frac{\Delta x}{2}$   $i = 1, ..., n-1$ ,  $W_{an} = w_{an} \frac{\Delta x}{2}$ . (7)

Figure 6(b) shows the free body diagram of bar i, which is affected by the normal force  $N_i$ . This force has horizontal and vertical force components  $H_i$  and  $V_i$ . The gradient of the bar is

$$k_i = \frac{V_i}{H_i} = \frac{y_i - y_{i-1}}{x_i - x_{i-1}}.$$
 (8)

If the loading of the arch is vertical as shown in Figure 5, the horizontal force is constant *H*.

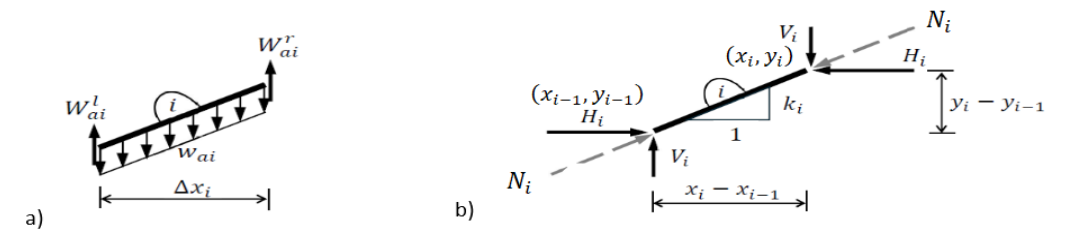


Figure 6. (a) Equivalent uniform bar load  $w_{ai}$  and corresponding bar end loads. (b) Free body diagram of bar i between the nodes i-1 and i.

The vertical force and moment equilibrium of the model with respect to point A give the support reaction  $V_A$  and the horizontal force H as:

$$V_A = \sum_{i=0}^{n} W_i$$
 and  $H = \frac{1}{h} \sum_{i=1}^{n} W_i x_i$  (9)

where  $W_i = W_{ai} + W_{di}$  at the base of hanger nodes and  $W_i = W_{ai}$  at arch nodes. Figure 7 shows the free body diagram of the arch nodes 0 and *i*. Vertical equilibrium of node 0 and *i* give the vertical forces

$$V_1 = V_A - W_0$$
 and  $V_{i+1} = V_i - W_i$   $i = 1, ..., n - 1$ . (10)

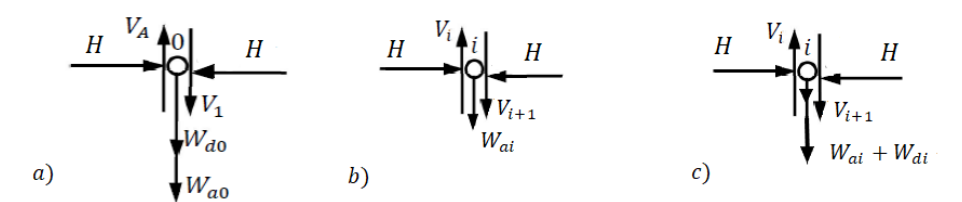


Figure 7. Free body drawing: (a) Arch base point 0, (b) Arch point *i* without hangers, (c) Arch point *i* with hangers.

The calculation process for the arch segment shown in Figure 5 begins with the predetermined deck weight. The equivalent nodal loads of the uniform deck load  $w_d$  are calculated by treating the deck as a simply supported beam between the hangers.

The support reaction  $V_A$  and the horizontal force H are then determined using Equations (9). The vertical forces of the arch are then calculated using Equations (10). The gradients of the arch bars are calculated using the following equation

$$k_i = \frac{V_i}{H} \quad i = 1, ..., n.$$
 (12)

The y-coordinates shown in Figure 6(b) of the nodes are determined using equations

$$y_0 = 0$$
 and  $y_i = y_{1-1} + k_i(x_i - x_{i-1})$   $i = 1, ..., n$ . (13)

In connection with constant stress arch, the distributed loads  $w_{ai}$  of the arch bars are determined based on the predefined constant stress  $\sigma_a$ . The cross-sectional area of bar i gets the form

$$A_{ai} = \frac{N_i}{\sigma_a},\tag{14}$$

where the normal force of the arch is

$$N_i = \sqrt{H^2 + V_i^2} = H\sqrt{1 + k_i^2}. (15)$$

The calculation process can be initiated based solely on the weight of the deck bars, when span length, height, and unit weights of the tied-arch materials and their stresses for permanent loads have been determined. The apex positions given in Equation (3) for the weightless arch can be used as the initial apex positions in the first iteration. This enables the initial y-coordinates and normal forces of the two weightless arch segments to be obtained. The arch bars can then be dimensioned using Equation (14). Their weight can then be applied in subsequent calculation rounds. The calculations then continue by varying the positions s and t to find the dimensions that yield an equal normal force t for both arch halves. The calculations show that three to five iterations are sufficient for practical design purposes.

# Example case

The example case is calculated for an arch length of 200 m and an arch rise of 60 m, with a difference in support line levels of 20 m. The arch is a steel structure and the compressive stress used is 75 MPa. The spacing of the hangers is determined by dividing the span by 20. The arch has been divided into 100 elements to calculate its coordinates, including those between the hangers.

The iterative calculation is initiated using the apex position of the weightless arch as given in Equation (3) which gives the dimension s of 110.102 m. When weight is added to the arch, the s value becomes 109.928 m. After iteration, the balance of the arch is obtained with a horizontal force H of 115.230w, where w is the vertical uniform unit weight of the deck. The weight of the tie is included in the deck weight w and hangers are assumed to be weightless. Figure 8 illustrates the form-found tied-arch, calculated as constant stress arch.

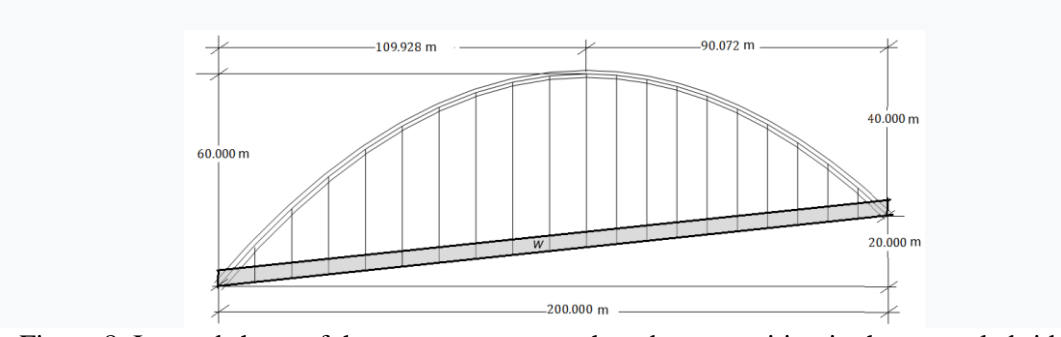


Figure 8. Iterated shape of the constant stress arch and apex position in the example bridge.

The analytical formulas for the apex position of a constant stress arch, subjected to the combined action of its own weight and a uniform vertical load can be found in reference [7]. Using the reference publication, the distance *s* can be calculated

$$s = \frac{\cos^{-1} e^{-\frac{\gamma h}{\sigma}}}{\cos^{-1} e^{-\frac{\gamma (h-d)}{\sigma}} + \cos^{-1} e^{-\frac{\gamma h}{\sigma}}} L,$$
 (16)

where the stress  $\sigma$  is the value used for dimensioning the arch and  $\gamma$  is the unit weight of the arch.

When the values  $\sigma = 75$  MPa,  $\gamma = 0.0785$  MN/m<sup>3</sup>, h = 60 m, d = 20 m and L = 200 m are applied to Equation (16), the distance s is found to be 109.929 m, which deviates only 1 mm from the iterated distance.

The value of the horizontal force H can be expressed as

$$H = \frac{\sigma \gamma w}{\left[ (\sigma/s) \cos^{-1} e^{-\frac{\gamma h}{\sigma}} \right]^2 - \gamma^2}.$$
 (17)

When the numeric example values are applied to Equation (17), the horizontal force H is found to be 115.240w. The value obtained by iteration is 115.230w.

The coordinates of the arch can be calculated as follows:

$$y = h + \frac{\sigma}{\gamma} \ln \cos \left( \sqrt{\kappa \gamma / \sigma} (x - s) \right), \tag{18}$$

where  $\kappa = w/H + \gamma/\sigma$ .

The shape obtained from analytical Equation (18) was verified against the results of a numerical, iterative calculation. The results reveal only minor deviations, which are understood to be caused by differences in the calculation models. The numerical model uses hangers spaced 10 meters apart, whereas the analytical calculation combines deck and arch loads over the entire arch.

## Comparison of anti-funicular arch shape to parabolic arch shape

Figure 9 shows the difference of the iterated constant stress arch and the weightless parabolic arch using the same apex position.

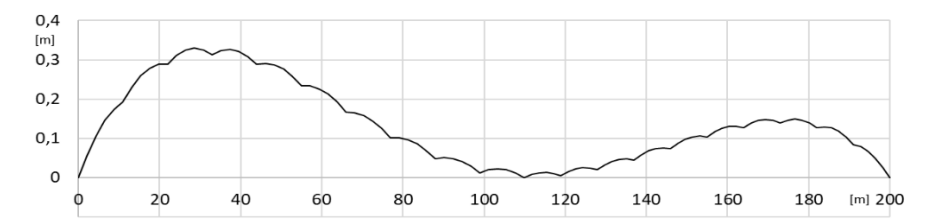


Figure 9. The difference of the shape of the constant stress arch to the weightless arch.

The largest difference is 0.33 metres. This difference is not noticeable to the naked eye on the real bridge, but it does indicate the need to find a moment-free form.

#### Asymmetry of the arch using vertical hangers

The shape of the arch is determined by the loads it must carry. If a vertical, uniform, constant load is applied, a parabolic shape is required for the momentless arch. The following section describes an arch with vertical hangers and an asymmetric arch shape resulting from a change in vertical load.

Figure 10 shows an arch composed of two parabolic semi-arches intersecting at the selected apex. The balanced anti-funicular parabolic arch requires the weight of the deck, tendons, hangers and arch rib to conform to a uniformly distributed constant load. Note that, in this case, the position of the apex has been selected, whereas in the previous case it was calculated.

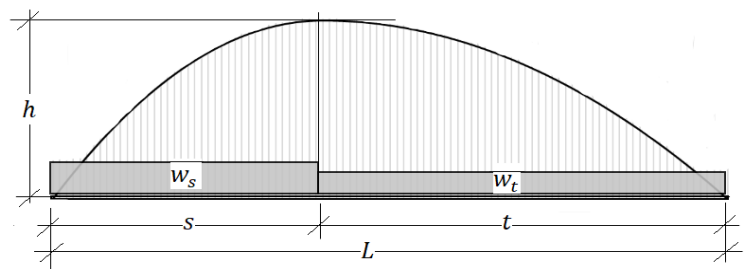


Figure 10. Parabolic arches.

Similarly to what was discussed above, the condition of equilibrium at the top of the arch requires the horizontal forces from both arch segments to be equal. Figure 11 shows the parabolic arch halves that meet this criterion.

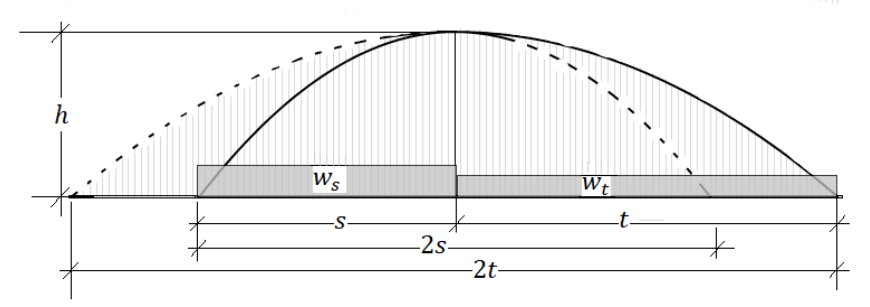


Figure 11. Equilibrium of the two half arches.

Using the symbols shown in Figure 11 the equilibrium requires that

$$H = \frac{w_s s^2}{2h} = \frac{w_t t^2}{2h}. (19)$$

Equation (19) leads to the ratio between the uniform loads as:

$$\frac{w_s}{w_t} = \frac{t^2}{s^2}. (20)$$

In practice, the load balancing could be achieved through the utilization of a combination of concrete and steel deck structures, with the weights corresponding to the arch geometry. Only limited asymmetry may be feasible in real bridges.

Equation (20) only provides a rough approximation because it does not consider the weight of the arch or the hangers. To eliminate bending moments when real permanent loading is taken into account, a more accurate arch shape is needed. This leads to iterative calculations. It is also worth considering that an asymmetric tied arch with vertical hangers and additional weight may not be aesthetically pleasing or economically viable.

# Asymmetric arch using inclined parallel hanger cables

When the vertical hangers of a tied-arch are changed to an inclined position, bending moments are generated. The momentless shape of the arch can be calculated to correspond to this change. The load-bearing principle remains the same: the hangers carry the weight of the beam itself. Introducing this change modifies both the arch's shape and the position of the apex.

# Asymmetric shape of arch with weightless arch

It has been demonstrated that an aesthetically pleasing and asymmetric shape can be achieved without any additional weight as demonstrated above. This can be accomplished by employing inclined parallel hanger cables. The subsequent discussion will elaborate on this method.

Figure 12 shows a diagram of a weightless, asymmetric tied-arch structure. The equivalent nodal loads  $W_{di}$  of the deck are equal to the uniform deck load  $w_d$ . The span length of the arch is denoted L and the height of the arch h. The x-coordinates of the hangers on the deck are denoted by  $x_{di}$ .

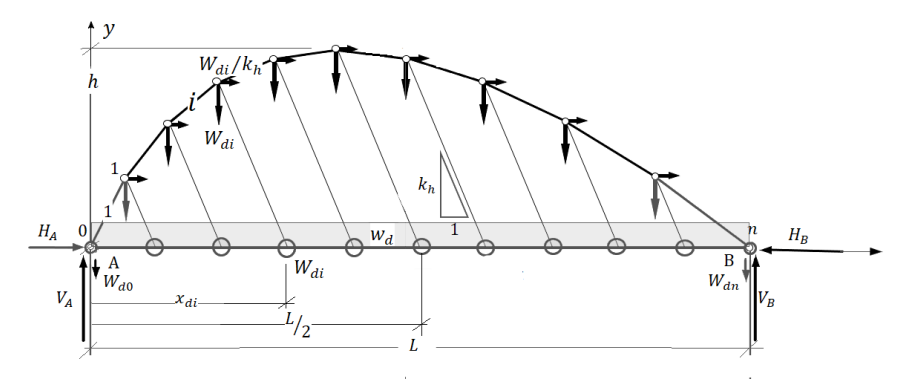


Figure 12. Asymmetric tied-arch with inclined hangers and weightless arch.

The support reactions  $V_A$  and  $V_B$  can be found by applying the principle of moment equilibrium at points A and B, and are analogous to the reactions of the simply supported beam. The support reaction can be calculated as follows:

$$V_A = V_B = \frac{w_d L^2}{2}, \qquad H_C = \frac{w_d L^2}{8h}, \qquad H_A = H_C - \sum_{i=1}^{n-1} \frac{W_{di}}{k_h}.$$
 (21)

Conversely, equilibrium will be achieved if the tied-arch is split into segments along the line from the apex to the middle of the span. This method is applied later in finding the shape of constant stress archs. Figure 13 illustrates the principle of the divided arch segments in balance.

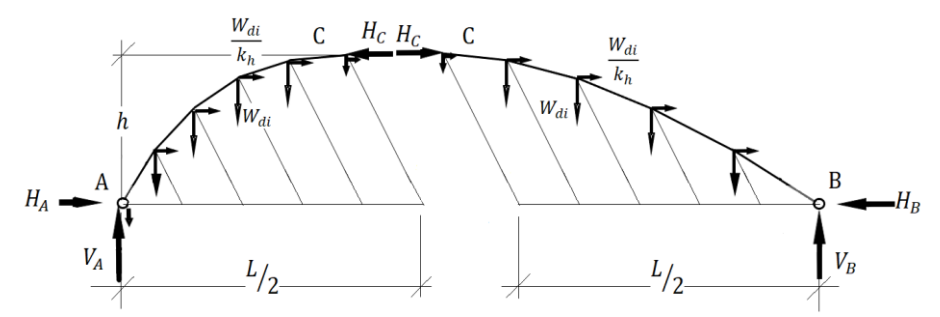


Figure 13. Balance of split tied-arch segments with weightless arch.

When the deck load is assumed to be a uniform load, the support reactions  $V_A$  and  $V_B$  are equal, as are the horizontal forces  $H_C$  and at the top of the arch.

Vertical and horizontal equilibrium of the nodes 0, i = 1, ..., n - 1 (see Figure 14) give

$$V_1 = V_A - W_{d0}, \qquad V_{i+1} = V_i - W_{di}, i = 1, ..., n - 1.$$
 (22)

$$H_1 = H_A$$
,  $H_{i+1} = H_i + \frac{W_{di}}{k_h}$ ,  $i = 1, ..., n - 1$ . (23)

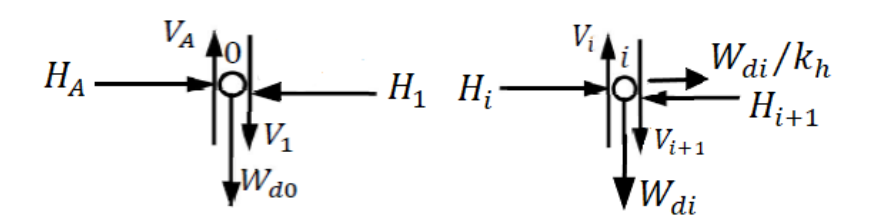


Figure 14. Free body diagram of the nodes 0 and  $i = 1 \dots n - 1$  of the arch.

The gradients  $k_i$  of the bars are

$$k_i = \frac{V_i}{H_i}$$
  $i = 1, ..., n.$  (24)

Equations (22), (23), and (24) provide the vertical and horizontal force resultants and the gradients of the bars. The coordinates of the nodes are obtained by solving for the intersection points of the axial and hanger forces.

$$\begin{cases} y - y_{i-1} = k_i(x - x_{i-1}) \\ y = -k_h(x - x_{di}). \end{cases}$$
 (25)

Figure 15 demonstrates the intersection lines of the hangers and axial force vector lines.

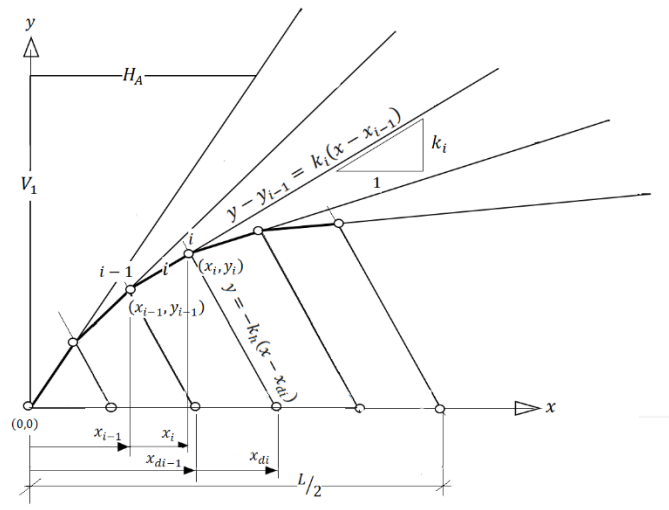


Figure 15. Demonstration of the solution of the weightless arch coordinates.

The coordinates of the intersection are

$$x_i = \frac{-y_{i-1} + k_i x_{i-1} + k_h x_{di}}{k_i + k_h}, \quad y_i = k_h (x_{di} - x_i).$$
 (26)

The summation of the vectors over the arch has been illustrated in Figure 16.

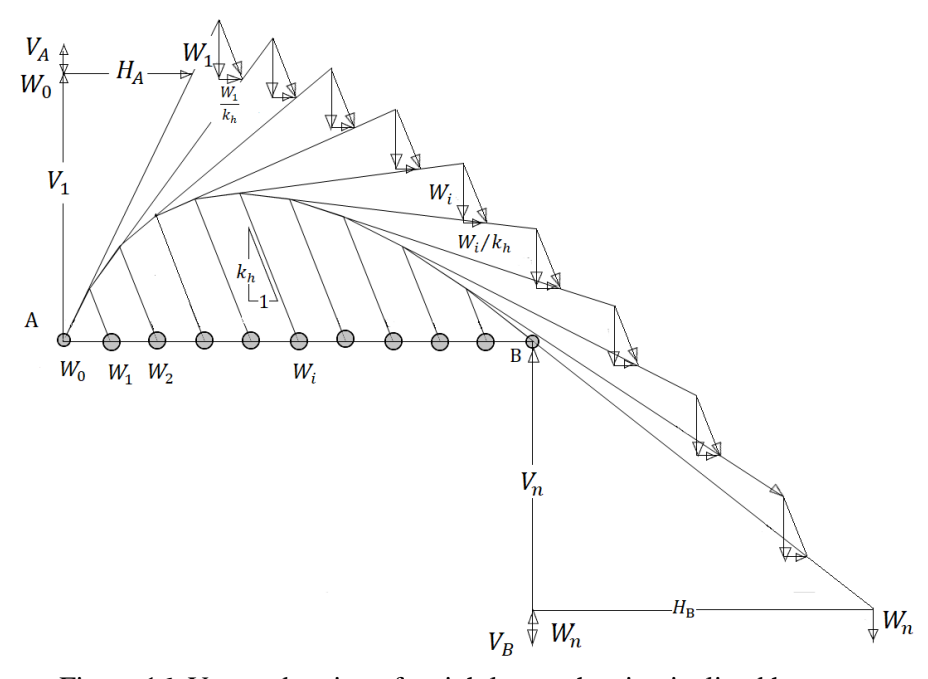


Figure 16. Vector drawing of weightless arch using inclined hangers.

Further demonstrations in Figure 17 illustrate the shape of the arch when the gradient  $k_h$  of the hangers varies from vertical to 1.00. The span-to-rise ratio L/h of the arches is in the examples is 4.0.

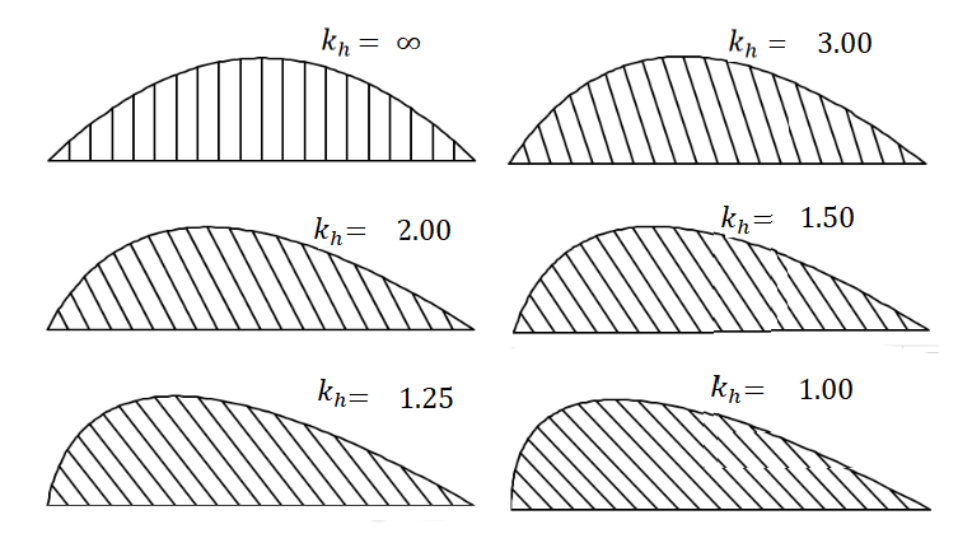


Figure 17. Example of shapes of arches by varying the gradient of the hangers. The span-to-rise ratio is 4.0.

The nodal coordinates of a weightless arch with inclined, parallel hangers and a uniform deck load can also be calculated using the analytic equations (27) and (28), as given in Reference [8]. The variables that are required for the calculation are illustrated in Figure 18.

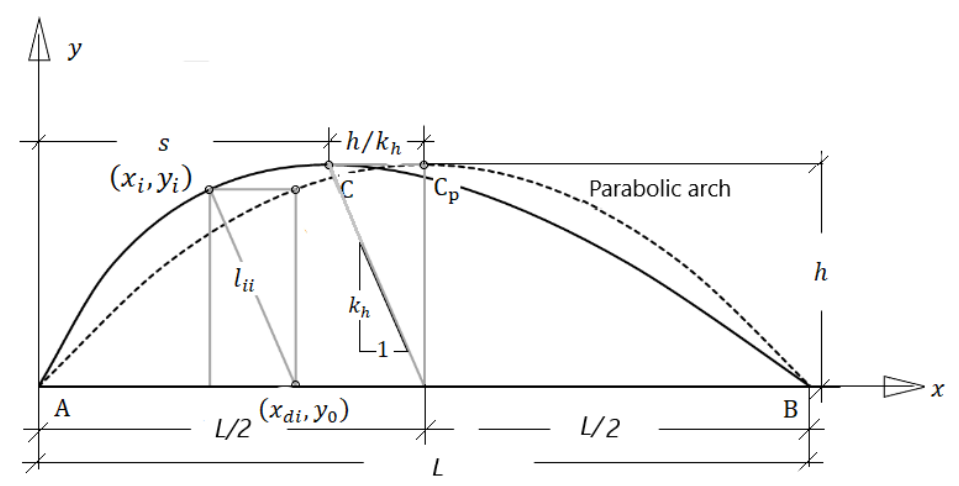


Figure 18. Coordinates of asymmetric weightless arch with inclined parallel hangers.

The height coordinate  $y_i$  of the arch at the upper end of the hanger is determined by the lower end coordinate  $x_{di}$  of the inclined hanger as:

$$y_i = \frac{4hx_{di}}{L^2}(L - x_{di}). (27)$$

The corresponding coordinate  $x_i$  of the arch is expressed as follows:

$$x_i = x_{di} + \frac{y_i}{k_h},\tag{28}$$

where  $k_h$  is the inclination gradient of the hangers. The inclination has positive value when the y-coordinate increases in proportion of to the increase of the x-coordinate, and negative value when the y-coordinate decreases.

# Asymmetric arch shape including the weight of arch

Assuming a uniform, constant deck weight supported by inclined hangers, as well as a constant weight distributed along the arch, an analytical solution for the shape results in a third-order differential equation [8]. Using a numerical iterative vector calculation method, it is possible to determine the arch's constant stress shape and the axial forces in the arch, tie, and hangers. The cross-sections and respective weights are dimensioned based on the selected stresses. The height of the arch and the inclination  $k_h$  of the hangers are pre-selected in the proposed calculation.

The calculation method is based on the same principle as that shown above for the weightless arch. The nodal loads of the arch include equivalent nodal loads  $W_{ai}$  corresponding to the weights  $w_{ai}$  of the arch bars, and the components  $W_{di}$  and  $W_{di}/k_h$  of the deck loads. Figure 19 shows the two parts of the arch. In the following, the self-weight of the tie is assumed to be included in the weight of the deck, and the hangers are assumed to be weightless. However, the calculation method allows these to be included in the analysis, if necessary.

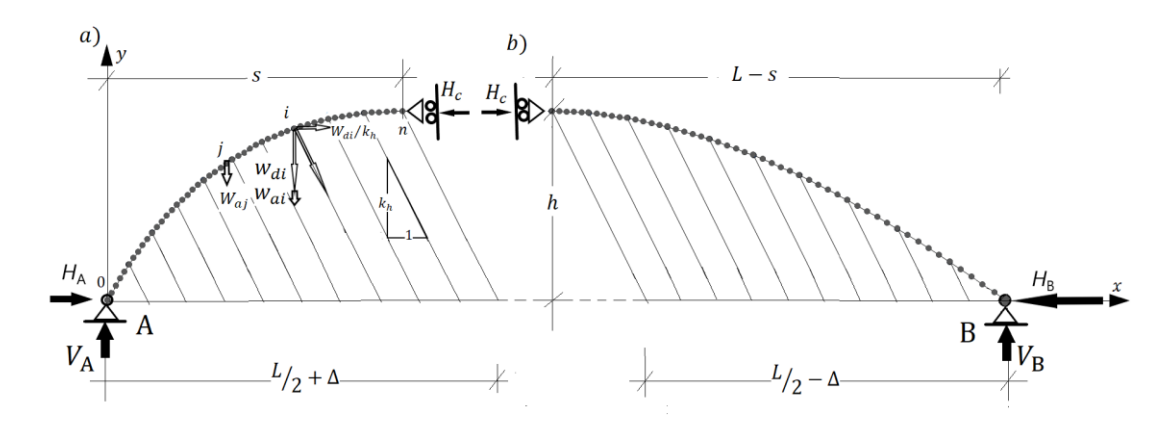


Figure 19. Free body drawing of the (a) left and (b) segments.

The equations used in the analysis of the left arch segment are given in the following. The *x*- coordinates of the deck nodes are

$$x_{di} = i\Delta x_d \quad i = 0, \dots n, \tag{29}$$

where

$$\Delta x_d = \frac{\frac{L}{2} + \Delta}{n}.\tag{30}$$

The horizontal support reaction at the apex C is

$$H_c = \frac{w_d \left(\frac{L}{2} + \Delta\right)^2}{2h} + \frac{1}{h} \sum_{i=1}^n W_{ai} x_i.$$
 (31)

The vertical and horizontal support reactions at point A are obtained from the equations

$$V_A = w_d \left(\frac{L}{2} + \Delta\right) + \sum_{i=0}^n W_{ai}, \qquad V_A = H_c - \frac{w_d \left(\frac{L}{2} + \Delta\right)}{k_h}.$$
 (32)

The horizontal and vertical forces on of the arch bar 1 are

$$H_1 = H_A, \quad V_1 = V_A - W_{do} - W_{ao}.$$
 (33)

The horizontal and vertical forces of the arch bars  $i = 2 \dots n$  are obtained from

$$H_{i+1} = H_i$$
, node without hanger  $H_{i+1} = H_i + \frac{W_{di}}{k_h}$ , node  $i$  with hanger  $i = 1 \dots n - 1$ , (34)

and

$$V_{1+1} = V_1 - W_{ai}$$
, node i without hanger  $V_{i+1} = V_i - W_{di} - W_{ai}$ , node i with hanger  $i = 1 \dots n - 1$ . (35)

The calculation then continues using Equations (24) and (26). The analysis of the right arch segment is very similar and is not presented here. At the beginning, only the deck load is given and the value of  $\Delta = 0$ . The left and right segments a) and b) are analysed. When the weight of arch, based on the axial forces and given stress, is added, different values for  $H_c^a$  and  $H_c^a$  are resulted. In the iteration process the value  $\Delta$  is adjusted so that  $H_c^a = H_c^a$  finally holds. The right segment can be calculated in Excel by simply changing the sign of the hanger inclination from positive to negative.

Figure 20 presents a free body diagram of the arch's base nodal point, alongside corresponding diagrams of the nodal points of the arch, both with and without the inclined hanger.

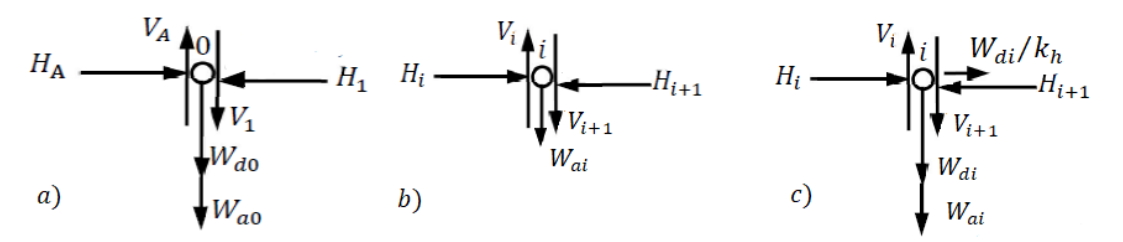


Figure 20. Free body drawing: (a) Arch base point 0, (b) Arch point *i* without hangers, (c) Arch point *i* with hangers.

Figure 21 illustrates the final shape of an iterated, constant stress, asymmetric tiedarch. The thickness of the arch drawn corresponds to the cross-sectional area of the arch. The change  $\Delta$  of the apex position due to weight of the arch bars is shown in the figure. Further calculations are demonstrated in the following example case.

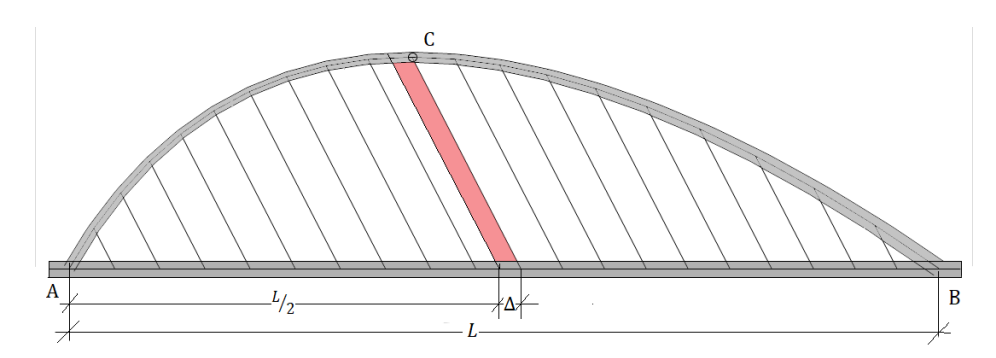


Figure 21. Constant stress, asymmetricarch and the change of apex position.

# Convergency of arch shape

The convergence of the arch shape is fast. After calculating the weightless, moment-free shape of the arch, only three to five iterations are required to achieve reasonably good results. The most significant change in the shape coordinates occurs when the weight of the arch is added to the arch for the first time. In the example bridge, the change in coordinates after the fourth iteration was found to be less than one millimetre. The arch shape changed in the *x*- and *y*-directions.

## Example calculations

In the example calculated, the arch length is 200 m and the arch rise is 50 m. The deck weight used is  $0.250 \, \text{MN/m}^3$ . The inclination  $k_h$  of the hangers is 2 and the arch is a steel structure with a compressive stress of 75 MPa for permanent loads. Figure 22 shows the side view of the arch and the cross-section of the deck structure. The arches are vertically aligned in the same plane as the stiffening girders, with a spacing of 20 m between the arches.

The arch is calculated as a constant stress arch. The cross-sectional area of the arch is 0.190 m² at the top, 0.215 m² at the steeper end base, and 0.330 m² at the base of the shallower side. The smallest cross-sectional area, 0.173 m², is 48.36 m from the bearing line of the steeper end.

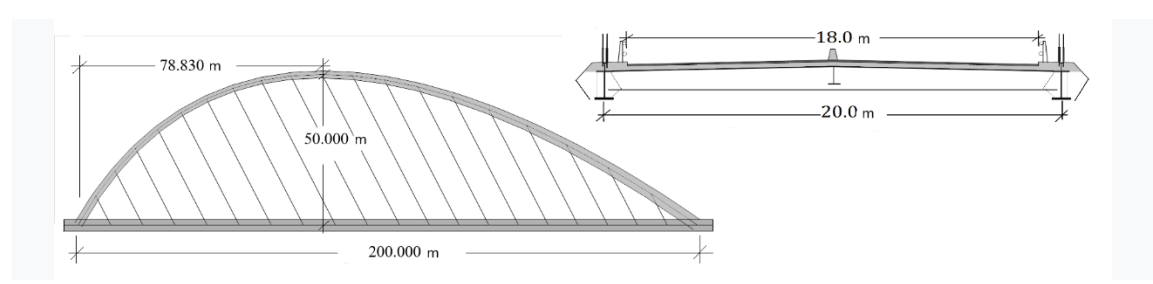


Figure 22. Constant stress, asymmetric tied-arch and the cross-section of the deck.

The position of the apex in the weightless arch has shifted by 3.83 m, from a distance of 75.0 m to a distance of 78.83 m, as a consequence of the weight of the arch.

The calculation for comparison purposes was carried out for the corresponding symmetrical constant stress arch with the same span, height, deck load and stresses. The cross sections of the stiffening girders in both bridges were assumed to be the same. The ratio between the hanger cross-sections of the asymmetrical arch compared to the symmetrical arch cross-sections is equal to  $\sqrt{1 + k_h^2}/k_h$ . Figure 23 shows the cross-sectional areas of both arches and Figure 24 the corresponding tie forces.

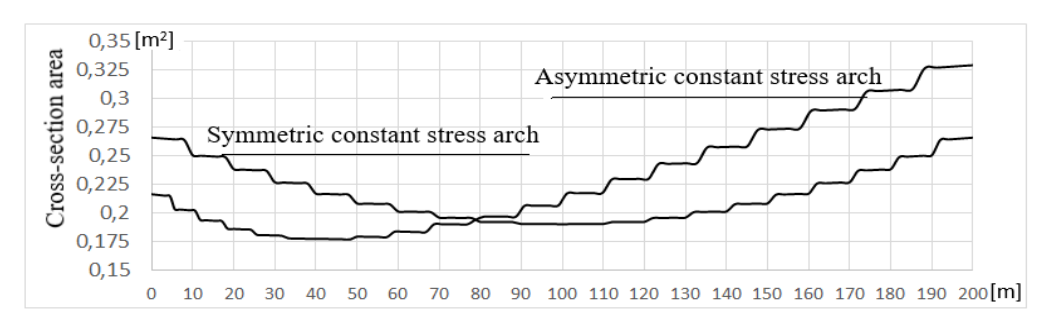


Figure 23. Cross-section areas of the asymmetric arch and corresponding symmetric arch.

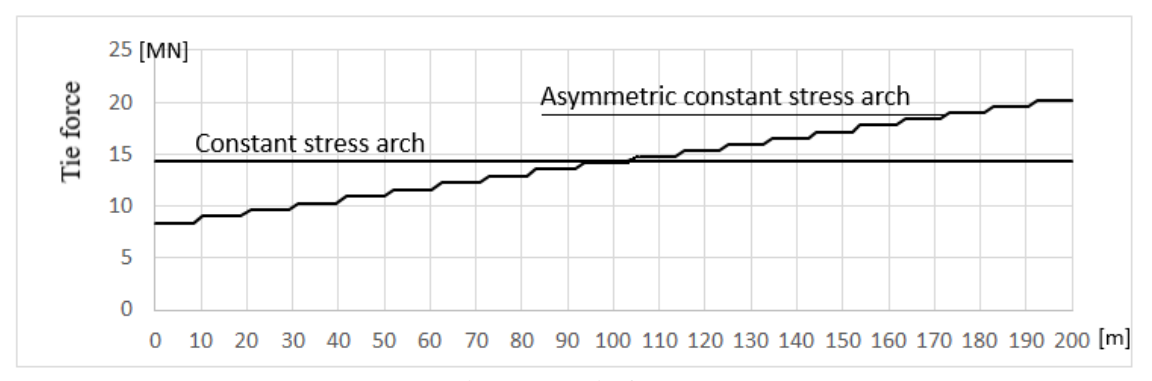


Figure 24. Tie forces.

## Verification using FEM calculations

#### Verification calculation for permanent loads

The results of the iterative calculations were verified using the finite element method (FEM), applying the geometry and cross-sections of the iterated structure. The Lusas programme calculations were performed using a two-dimensional structure and a three-dimensional beam element. The arch geometry and all the necessary structural data were obtained from the aforementioned iterative calculations. The equivalent deck node loads were calculated as support reactions of the continuous girder. It was assumed that the joint between the deck girder and arch was hinged.

The verification calculation for permanent loads was carried out using rigid members. This condition was met in the finite element verification calculation. The hangers were prestressed to forces determined by the weight of the deck. Arch compression and tie

elongation were eliminated by using high axial stiffness. Figure 25 shows the bending moments of the structure for permanent loads.

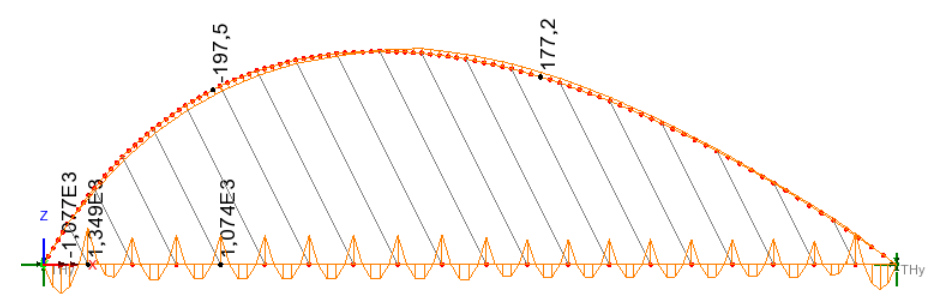


Figure 25. Results of the bending moments for one arch [kNm], using FEM calculation in the asymmetric constant stress arch using rigid members.

The results of the verification calculation show the bending moments in the stiffening girder of the continuous girder. Small bending moments are observed in the arch. This is due to slight discrepancies in the hanger forces, calculated using the finite element method and the numerical method.

#### Bending moments of traffic loads due to asymmetric shape

The asymmetric shape raises questions about the structure's tendency to exhibit undesirable behaviour. To illustrate this, the maximum and minimum bending moments for traffic load in the arch and tie girder were compared for the asymmetric arch and the corresponding symmetric arch.

The traffic load applied was the traffic load model LM1 from Eurocode EN 1991-2. The Finnish national factors for the LM1 load model (NA EN 1991-2) give a tandem load of 2 x 300 kN on the first two load lines, and surface loads for the load lines of 9 kN/m $^2$ , 6 kN/m $^2$ , and 3 kN/m $^2$ . The width of the load lines is 3 m, and they are applied from the edge of the bridge parapets. The load model LM1 was simplified to line loads in the maximum and minimum bending moment calculations. A load effect on the 2D arch was approximated with a linear influence line in the transverse direction of the deck. Figure 26 shows the nominal eccentric traffic load combination on the bridge deck.

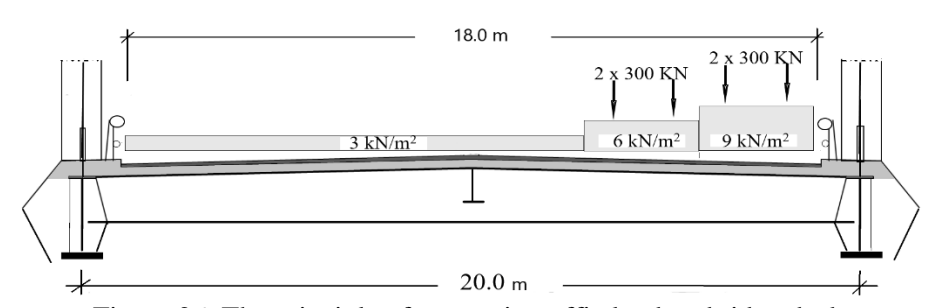


Figure 26. The principle of excentric traffic load on bridge deck.

Figure 27 shows the minimum and maximum bending moments in the girder and arch of the asymmetric bridge. Figure 28 shows the corresponding bending moments for the symmetric bridge, which were calculated for comparison purposes.

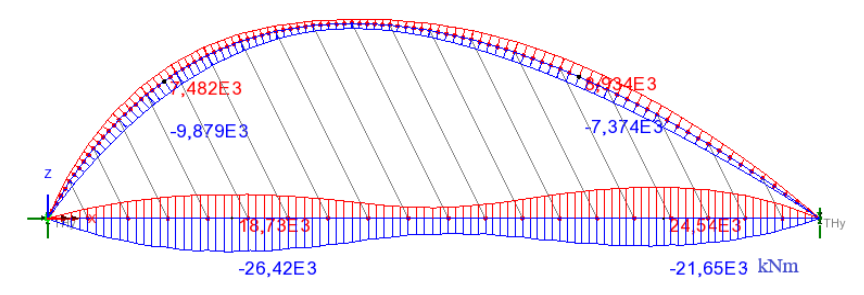


Figure 27. Bending moment field due to the traffic load in the asymmetric bridge, for one arch and stiffening girder.

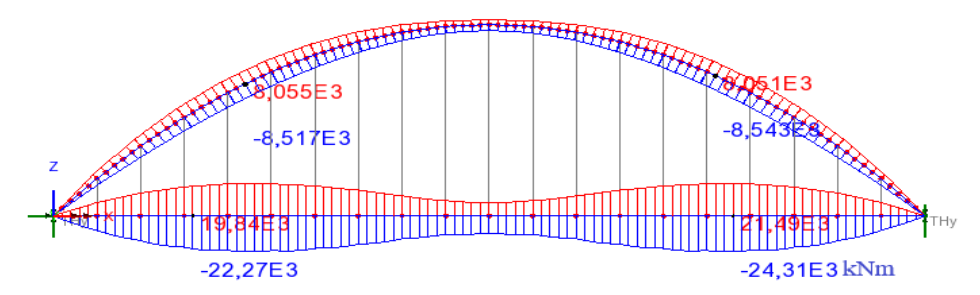


Figure 28. Bending moment field due to the traffic load in the corresponding symmetric bridge, for one arch and stiffening girder.

Figures 27 and 28 reveal that the influence of asymmetry to the bending moments of traffic loads is rather small.

# Load-bearing materials and costs according to hanger inclination

The asymmetric bridges studied had the following dimensions: a span of 200 metres and an arch rise of 50 metres. The inclination  $k_h$  of the hanger cables was varied from an asymmetric constant stress to a vertical, symmetric arch, with inclination values of 1.0, 1.25, 2.0, 2.5, 3.0, 3.5, 4.0 and infinity. Each arch was iterated to constant stress. The iterative vector calculation resulted in the forces of the arch, tie tendons and hangers. The quantity of material required for the arch was calculated using a compressive stress of 75 MPa. The material quantities for the tie tendons and hangers were calculated using high-strength steel with stress values of 600 MPa and 400 MPa, respectively. Figure 29 illustrates the quantities of steel in the arches, tie tendons and hangers according to the inclination of the hangers. This calculation only considers permanent loads and assumes that the effect of traffic loads is equal. Further studies may be required.

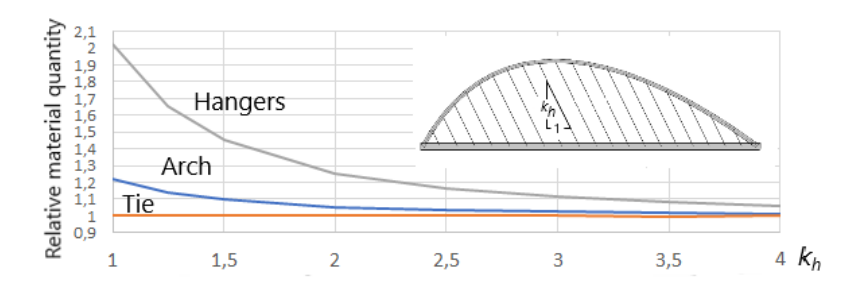


Figure 29. Relative quantities of each load-bearing material in relation to hanger inclination in the example. The span-to-rise relation l/h = 4.0.

Figure 30 illustrates the relative cost of the load-bearing materials in the constant stress, inclined hanger, asymmetric tied-arch bridge compared to the vertical hanger, symmetric tied-arch bridge. This calculation is based on material quantity data obtained for iterated constant stress arches and assumes relative unit costs of 1.0, 3.0 and 5.0 for the arch, tendons, and hangers, respectively.

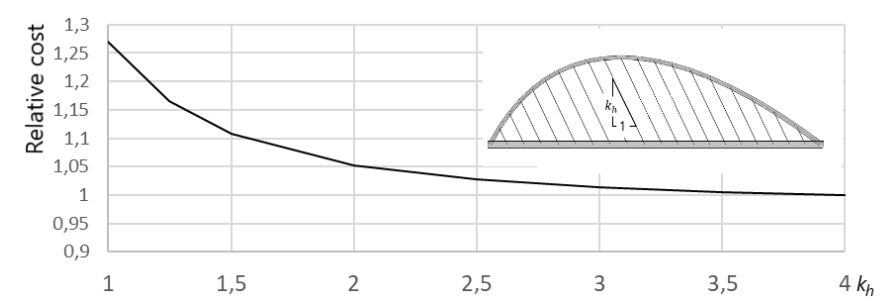


Figure 30. Relative load-bearing material costs in the example in relation to hanger inclination, l/h = 4.0.

It would appear that the impact of the asymmetric shape on cost is relatively modest when inclined hangers are used.

#### Asymmetric network tied-arch bridge

The reduction in the amount of material used in network arch bridges has led to a significant increase in the utilisation of this type of bridge. In addition, recent developments in carbon fibre hangers represent a further potential avenue for optimising this type of bridge.

Previously, it was accepted that no further adjustments were required to the shape of the arch or to the prestressing of the hanger forces in network arch bridges, as the bending moments without adjustment were relatively small, especially compared to those of a vertical hanger arch bridge [9]. Nevertheless, there may be scope for further optimisation of the shape of both symmetrical and asymmetrical network arch bridges [10].

The above-presented method for a parallel inclined hanger can be used to calculate the anti-funicular shape of an asymmetric network tied-arch bridge. Figure 31 shows a simplified approach in which the parallel hangers (AB) are replaced by two network hangers (AC and AD). This results in hanger loads and an arch shape that are equivalent to those using parallel hangers.

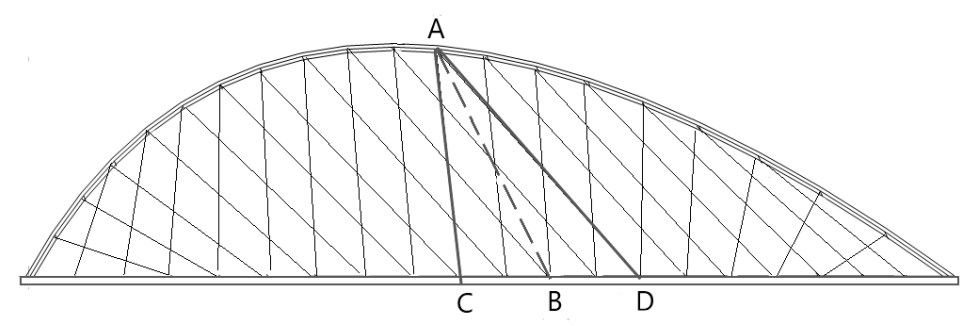


Figure 31. Modification from parallel inclined hangers to network hangers.

This means that the arch has the same momentless geometry as that calculated with parallel hangers. However, bending moments are induced in the stiffening girder. In practice, these moments are small and of no further interest.

#### Conclusion

Inevitably, asymmetry leads to increased costs. These costs can be mitigated effectively by designing the arch shape, selecting the arch height, and adjusting the hanger cables through prestressing. A constant stress arch shape is recommended.

An important starting point in designing an asymmetric arch is determining the location of the arch apex. Splitting the arch in two segments makes possible spreadsheet calculations using rigid body calculations.

Using an iterative calculation method involving basic statics and vector algebra to find the momentless, constant stress shape solution for permanent loads on the arch gives a sound basis for a balanced structure. The studies and prepared calculations show that convergence takes place to an accuracy of a few millimetres already after four iteration rounds. In practice, further minor adjustments are done using the real material properties.

For an asymmetrical, constant stress, tied-arch bridge with a gradient of 2 for the parallel hangers and a span-to-rise ratio of 4, the total cost of the arch, tendons, and hangers increases by around 5% compared to a corresponding vertical hanger tied-arch. This is less than expected as the arch's shape is relatively strongly asymmetric.

Calculations for various hanger gradients have demonstrated that introducing parallel inclined hangers creates an aesthetically attractive and cost-effective structure. The calculations show that hanger inclination has a relatively small effect on the structure's bending moments due to traffic loads. The introduction of a network system of hangers is an additional improvement that requires further study.

#### References

- [1] P. Menetray. The Integrative Design Method for Bridges, Structural Engineering International, SEI Volume 28, Number 3, 2018.
- [2] R. Gerhardt, K-E. Kurrer & G. Pichler. The methods of graphical statics and their relation to the structural form. Proceedings of the First International Congress on Construction History, 2003.

- [3] E. Järvenpää, Q. Tung. Simple cost comparison between bridges and cable-stayed bridges. MATEC Web Conferences, 258, SCESCM 2018. https://doi.org/10.1051/matecconf/201925802015
- [4] P. Pulkkinen, S. Hopf & A. Jutila. Conceptual Design of the Chenab Bridge in India. Science direct, 2012. https://doi.org/10.1016/j.proeng.2012.07.078
- [5] B. Kaiming, H. Hong, & R. Wei-Xin. Seismic Response of a Concrete Filled Steel Tubular Arch Bridge to Spatially Varying Ground Motions Including Local Site. Advances in Structural Engineering, 16(10:171818), 2013. https://doi.org/10.1260/1369-4332.16.10.1799
- [6] T. Van Mele & P. Block. Algebraic graph statics. Computer-Aided Design, 53, 104–116, 2014. https://doi.org/10.1016/j.cad.2014.04.004
- [7] W. Lewis. Constant stress arches and their design space. Proceedings of the Royal Society A, 2022. https://doi.org/10.1098/rspa.2021.0428
- [8] W. Wang, S. Li & K. Chen. Variant bowstring arch bridge. China Journal of Highway and Transport, 9(1), 1996, 45–50.
- [9] B. Zwingmann, S. Marx & F. Schanack. Asymmetric network arch bridges. Structure and Architecture- Cruz (Ed.). Taylor & Francis Group, London, ISBN 978-0-415-49249-2.
- [10] U. Morf. Optimisation of Network Bridges, Arch Shape, Network Pattern and Density. ETHZ, 2020. Concrete Structures and Bridge Design. www.kaufmann.ibk.ethz.ch

Esko Järvenpää Civil Engineering Research Unit, Faculty of Technology, University of Oulu Pentti Kaiteran katu 1, 90570, Oulu, Finland esko.jarvenpaa@oulu.fi

Anssi Laaksonen Tampere University PL600, 33101, Tampere, Finland anssi.laaksonen@tuni.fi